
Direct Estimation of Differences in Causal Graphs

Yuhao Wang¹ Chandler Squires¹ Anastasiya Belyaeva¹ Caroline Uhler¹

Abstract

We consider the problem of estimating the differences between two causal directed acyclic graph (DAG) models given i.i.d. samples from each model. This is of interest for example in genomics, where large-scale gene expression data is becoming available under different cellular contexts, for different cell types, or disease states. Changes in the structure or edge weights of the underlying causal graphs reflect alterations in the gene regulatory networks and provide important insights into the emergence of a particular phenotype. While the individual networks are usually very large, containing high-degree hub nodes and thus difficult to learn, the overall change between two related networks can be sparse. We here provide the first provably consistent method for directly estimating the differences in a pair of causal DAGs without separately learning two possibly large and dense DAG models and computing their difference. Our two-step algorithm first uses invariance tests between regression coefficients of the two data sets to estimate the skeleton of the difference graph and then orients some of the edges using invariance tests between regression residual variances. We demonstrate the properties of our method through a simulation study and apply it to the analysis of gene expression data from ovarian cancer and during T-cell activation.

1. Introduction

Directed acyclic graph (DAG) models, also known as Bayesian networks, are widely used to model causal relationships in complex systems. Learning the *causal DAG* from observations on the nodes is a fundamentally important problem across disciplines including computational biology, epidemiology, sociology or economics (Friedman et al., 2000;

Pearl, 2000; Robins & Hernan, 2000; Spirtes et al., 2000). A variety of causal inference algorithms based on observational data have been developed; see for example the prominent PC (Spirtes et al., 2000) and GES (Meek, 1997) algorithms among others (Tsamardinos et al., 2006; Solus et al., 2017). However, it was recently shown that causal inference methods require very restrictive assumptions, which limit their applicability to relatively small and sparse graphs (Uhler et al., 2013). In particular, theoretical analysis of the PC (Kalisch & Bühlmann, 2007) and GES (Van de Geer & Bühlmann, 2013; Nandy et al., 2015) algorithms have shown that these methods are usually not consistent in the high-dimensional setting, i.e. when the number of nodes is of the same order or exceeds the number of samples, unless given highly restrictive assumptions including on the sparsity and the maximum degree of the underlying DAG.

The presence of high degree hub nodes is a well-known feature of networks across disciplines (Barabási & Oltvai, 2004; Barabási et al., 2011), which limits the direct applicability of causal inference algorithms in complex systems. However, in many applications, full recovery of the underlying causal DAG might not be necessary. Often the object of interest is to detect changes in the causal relations between two related networks. For example, in the analysis of EEG signals it is of interest to detect neurons or different brain regions that interact differently when the subject is performing different activities (Sanei & Chambers, 2013). In addition, genes may interact with each other in different ways or have different interaction targets under different cellular contexts or disease states (Pimanda et al., 2007; Hudson et al., 2009). Due to recent technological advances that allow the collection of large-scale EEG or single-cell gene expression data sets in different contexts there is a growing need for methods that can accurately identify differences in the underlying regulatory networks and thereby provide key insights into the underlying system (Pimanda et al., 2007; Hudson et al., 2009). The limitations of causal inference algorithms for accurately learning large causal networks with hub nodes and the fact that the difference of two related networks is often sparse call for methods that directly learn the difference of two causal networks without having to estimate each network separately.

This problem has been considered previously in the *undirected* setting. Two recent methods that directly learn the dif-

¹Laboratory for Information and Decision Systems and Institute for Data, Systems and Society, Massachusetts Institute of Technology, Cambridge, MA, USA. Correspondence to: Caroline Uhler <cuhler@mit.edu>.

ference of two *undirected graphical models* are KLIEP (Liu et al., 2014) and DPM (Zhao et al., 2014); Liu et al. (2017) provide a review and comparison of these methods. They have also been applied in genomics for learning differential gene association (i.e., undirected) networks from gene expression data (Zhao et al., 2014). However, for example for medical applications, analyzing the undirected setting is insufficient. Only a causal (i.e., directed) network provides insights into the effects of interventions such as knocking out a particular gene. In this paper we provide to our knowledge the first provably consistent method for directly inferring the differences between pairs of causal DAG models that does not require learning each model separately.

The remainder of this paper is structured as follows: In Section 2, we set up the notation and review related work with respect to learning causal DAG models and differences of graphical models. In Section 3, we present our algorithm for directly estimating the difference of causal relationships and in Section 4, we provide consistency guarantees for our algorithm. In Section 5, we evaluate the performance of our algorithm on both simulated and real datasets including gene expression data from ovarian cancers and T-cell activation.

2. Preliminaries and Related Work

2.1. Causal DAG models

Let $\mathcal{G} = ([p], A)$ be a DAG with node set $[p] := \{1, \dots, p\}$ and arrow set A . Without loss of generality assume that the nodes of \mathcal{G} are topologically ordered, meaning that if $i \rightarrow j$ in \mathcal{G} then $i < j$. To each node i we associate a random variable X_i and let \mathbb{P} be a joint distribution over the random vector $X = (X_1, \dots, X_p)^T$. In this paper, we consider the setting where the causal DAG model is given by a *linear structural equation model (SEM) with additive noise*, i.e.,

$$X = B^T X + \epsilon$$

where B is a strictly upper triangular matrix, known as the *autoregressive matrix*, consisting of the edge weights of \mathcal{G} , i.e., $B_{ij} \neq 0$ if and only if $i \rightarrow j$ in \mathcal{G} and $\epsilon = (\epsilon_1, \dots, \epsilon_p)^T$ is random noise. We assume that $\mathbb{E}[\epsilon] = 0$ and that $\epsilon_i \perp\!\!\!\perp \epsilon_j$ for all $i \neq j$ meaning that there are no latent confounders. Let σ_i denote the variance of the noise term ϵ_i , and let $\Omega := \text{diag}(\sigma_1^2, \dots, \sigma_p^2)$ be the covariance of ϵ . We denote by Σ the covariance matrix of X and by Θ its inverse, known as the *precision matrix*. A short computation yields that

$$\Theta = (I - B)\Omega^{-1}(I - B)^T,$$

and hence by multiplying out we obtain

$$\begin{aligned} \Theta_{ij} &= -\sigma_j^{-2} B_{ij} + \sum_{k>j} \sigma_k^{-2} B_{ik} B_{jk}, & \forall i \neq j, \\ \Theta_{ii} &= \sigma_i^{-2} + \sum_{j>i} \sigma_j^{-2} B_{ij}^2, & \forall i \in [p]. \end{aligned} \quad (1)$$

This shows that the support of Θ is given by the *moral graph* of \mathcal{G} , obtained by adding an edge between pairs of nodes that have a common child and removing all edge orientations.

By the *causal Markov assumption*, which we assume throughout, the missing edges in the moral graph encode a subset of the conditional independence (CI) relations implied by a DAG model on \mathcal{G} . In fact, a fundamental result about DAG models is that the complete set of CI relations is given by the *d-separations* that hold in \mathcal{G} (Lauritzen, 1996)[Section 3.2.2]; i.e., $X_i \perp\!\!\!\perp X_j \mid X_S$ in \mathbb{P} whenever nodes i and j are d-separated in \mathcal{G} given a set $S \subseteq [p] \setminus \{i, j\}$. The *faithfulness assumption* is the assertion that all CI relations entailed by \mathbb{P} are implied by d-separation in \mathcal{G} .

A standard approach for causal inference is to first infer CI relations from the observations on the nodes of \mathcal{G} and then to use the CI relations to learn the DAG structure. However, several DAGs can encode the same CI relations and therefore, \mathcal{G} can only be identified up to an equivalence class of DAGs, known as the *Markov equivalence class (MEC)* of \mathcal{G} , which we denote by $[\mathcal{G}]$. Verma & Pearl (1990) gave a graphical characterization of the members of $[\mathcal{G}]$; namely, two DAGs are in the same MEC if and only if they have the same *skeleton* (i.e., underlying undirected graph) and the same *v-structures* (i.e., induced subgraphs of the form $i \rightarrow j \leftarrow k$). $[\mathcal{G}]$ can be represented combinatorially by a partially directed graph with skeleton \mathcal{G} and an arrow for those edges in \mathcal{G} that have the same orientation in all members of $[\mathcal{G}]$. This is known as the *CP-DAG* (or *essential graph*) of \mathcal{G} (Andersson et al., 1997).

Various algorithms have been developed for learning the MEC of \mathcal{G} given observational data on the nodes, most notably the prominent GES (Meek, 1997) and PC algorithms (Spirtes et al., 2000). While GES is a score-based approach that greedily optimizes a score such as the BIC (Bayesian Information Criterion) over the space of MECs, the PC algorithm views causal inference as a constraint satisfaction problem with the constraints being the CI relations. In a two-stage approach, the PC algorithm first learns the skeleton of the underlying DAG and then determines the v-structures, both from the inferred CI relations. GES and the PC algorithms are provably consistent, meaning they output the correct MEC given an infinite amount of data, under the faithfulness assumption. Unfortunately, this assumption is very sensitive to hypothesis testing errors for inferring CI relations from data and violations are frequent especially in graphs with cycles in the skeleton (Uhler et al., 2013).

In this paper, we develop a two-stage approach, similar to the PC algorithm, for directly learning the difference between two DAG models \mathcal{G} and \mathcal{H} . Note that naive algorithms that separately estimate $[\mathcal{G}]$ and $[\mathcal{H}]$ and take their differences can only identify edges that appeared/disappeared and cannot identify changes in edge weights. Our algorithm

overcomes this limitation. In addition, we show in Section 4 that instead of requiring the restrictive faithfulness assumption on both DAGs \mathcal{G} and \mathcal{H} , consistency of our algorithm only requires assumptions on the (usually) smaller and sparser network of differences.

2.2. Differences of graphical models

Let $\mathbb{P}^{(1)}$ and $\mathbb{P}^{(2)}$ be a pair of linear SEMs with additive noise defined by $(B^{(1)}, \epsilon^{(1)})$ and $(B^{(2)}, \epsilon^{(2)})$. Throughout, we make the simplifying assumption that both $B^{(1)}$ and $B^{(2)}$ are strictly upper triangular, i.e., that the underlying DAGs $\mathcal{G}^{(1)}$ and $\mathcal{G}^{(2)}$ share the same topological order. This assumption is reasonable for example in applications to genomics, since genetic interactions may appear or disappear, but generally do not change directions. Hence $B^{(1)} - B^{(2)}$ is also strictly upper triangular and we define the *difference-DAG* of the two models by $\Delta := ([p], A_\Delta)$ with $i \rightarrow j \in A_\Delta$ if and only if $B_{ij}^{(1)} \neq B_{ij}^{(2)}$. Given i.i.d. samples from $\mathbb{P}^{(1)}$ and $\mathbb{P}^{(2)}$, our goal is to infer the DAG Δ . Similarly as for learning a causal DAG model separately, Δ is in general not completely identifiable, in which case we wish to identify the skeleton $\bar{\Delta}$ as well as a subset of arrows \tilde{A}_Δ .

A simpler task that has been considered previously is to learn differences of undirected graphical models. Let $\Theta^{(1)}$ and $\Theta^{(2)}$ denote the precision matrices corresponding to $\mathbb{P}^{(1)}$ and $\mathbb{P}^{(2)}$. Then the support of $\Theta^{(k)}$ consists of the edges in the undirected graphical models corresponding to $\mathbb{P}^{(k)}$. We define the *difference-UG* (undirected graph) Δ_Θ to be the undirected graph with edges $i - j$ if and only if $\Theta_{ij}^{(1)} \neq \Theta_{ij}^{(2)}$ for $i \neq j$. Various methods have been developed for directly inferring Δ_Θ in the Gaussian setting; see Liu et al. (2017) for a review. For example, *KLIEP* (Liu et al., 2014), which we will use to evaluate our method in Section 5, estimates the density ratio between $\mathbb{P}^{(1)}$ and $\mathbb{P}^{(2)}$, whose parameters in the Gaussian setting and more generally for quadratic exponential families correspond to the edges of the difference-UG. A major advantage of direct estimation methods such as KLIEP, that circumvent the need of separately estimating the parameters of $\mathbb{P}^{(1)}$ and $\mathbb{P}^{(2)}$, is that these methods do not require the undirected graphical models of $\mathbb{P}^{(1)}$ and $\mathbb{P}^{(2)}$ to be sparse as long as the difference-UG is sparse.

Methods such as KLIEP can be used as a first step towards estimating the difference-DAG Δ if the additive error ϵ is Gaussian: under genericity assumptions, the formulae for Θ_{ij} in (1) imply that if $B_{ij}^{(1)} \neq B_{ij}^{(2)}$ then $\Theta_{ij}^{(1)} \neq \Theta_{ij}^{(2)}$ and hence that the skeleton of the difference-DAG is a subgraph of the difference-UG, i.e., $\bar{\Delta} \subseteq \Delta_\Theta$. In the following section we present our algorithm showing how to obtain $\bar{\Delta}$ and determine some of the edge directions in Δ . We end this section with a piece of notation needed for introducing

our algorithm; we define the *set of changed nodes* to be

$$S_\Theta := \{i \mid \exists j \in [p] \text{ such that } \Theta_{i,j}^{(1)} \neq \Theta_{i,j}^{(2)}\}.$$

3. Difference Causal Inference Algorithm

In Algorithm 1 we present our *Difference Causal Inference (DCI)* algorithm for directly learning the difference between two linear SEMs with additive noise given i.i.d. samples from each model. Our algorithm consists of a two-step approach similar to the PC algorithm. The first step, described in Algorithm 2, estimates the skeleton of the difference-DAG by removing edges one-by-one. Algorithm 2 takes Δ_Θ and S_Θ as input. In the Gaussian setting or as a heuristic in the high-dimensional setting, KLIEP can be used to estimate these. In the Supplementary Material we also provide a constraint-based method that consistently estimates Δ_Θ and S_Θ in the low-dimensional setting for general additive noise models. Finally, Δ_Θ can also simply be chosen to be the complete graph with $S_\Theta = [p]$. These different initiations of Algorithm 2 are compared via simulations in Section 5. The second step of DCI, described in Algorithm 3, infers some of the edge directions in the difference-DAG. While the PC algorithm uses CI tests based on the partial correlations for inferring the skeleton and for determining edge orientations, DCI tests the invariance of certain *regression coefficients* across the two data sets in the first step and the invariance of certain *regression residual variances* in the second step. These are introduced in the following two definitions.

Definition 3.1. Given $i, j \in [p]$ and $S \subseteq [p] \setminus \{i, j\}$, let $M := \{i\} \cup S$ and let $\beta_M^{(k)}$ be the best linear predictor of $X_j^{(k)}$ given $X_M^{(k)}$, i.e., the minimizer of $\mathbb{E}[(X_j^{(k)} - (\beta_M^{(k)})^T X_M^{(k)})^2]$. We define the *regression coefficient* $\beta_{i,j|S}^{(k)}$ to be the entry in $\beta_M^{(k)}$ corresponding to i .

Definition 3.2. For $j \in [p]$ and $S \subseteq [p] \setminus \{j\}$, we define $(\sigma_{j|S}^{(k)})^2$ to be the *variance of the regression residual* when regressing $X_j^{(k)}$ onto the random vector $X_S^{(k)}$.

Note that $\beta_{i,j|S}^{(k)}$ and $\beta_{j,i|S}^{(k)}$ are in general not the same. Each entry in $B^{(k)}$ can be interpreted as a regression coefficient, namely

$$B_{ij}^{(k)} = \beta_{i,j|(\text{Pa}^{(k)}(j) \setminus \{i\})}^{(k)},$$

where $\text{Pa}^{(k)}(j)$ denotes the parents of node j in $\mathcal{G}^{(k)}$. This motivates using invariances between regression coefficients to determine the skeleton of the difference-DAG. Note that the partial correlations used by the PC algorithm for learning the skeleton of a causal DAG do not have such an interpretation.

The regression coefficients and residual variances need to be estimated from data. Hence, we need to design a hypothesis

Algorithm 1 Difference Causal Inference (DCI) algorithm

Input: Sample data $\hat{X}^{(1)}$ and $\hat{X}^{(2)}$.
Output: Estimated skeleton $\bar{\Delta}$ and arrows \tilde{A}_Θ of the difference-DAG Δ .
 Estimate difference-UG to obtain Δ_Θ and S_Θ ;
 Use Algorithm 2 to estimate $\bar{\Delta}$;
 Use Algorithm 3 to estimate \tilde{A}_Δ .

Algorithm 2 Estimating the skeleton of the difference-DAG

Input: Sample data $\hat{X}^{(1)}$ and $\hat{X}^{(2)}$, estimated difference-UG Δ_Θ , estimated set of changed nodes S_Θ .
Output: Estimated skeleton $\bar{\Delta}$.
 Set $\bar{\Delta} := \Delta_\Theta$;
for each edge $i - j$ in $\bar{\Delta}$ **do**
 repeat
 Choose $M \subseteq S_\Theta \setminus \{i, j\}$,
 if $\beta_{i,j|M}^{(k)}$ is invariant across $k = \{1, 2\}$ **then**
 delete $i - j$ in $\bar{\Delta}$;
 end if
 until edge $i - j$ has been deleted from $\bar{\Delta}$ or all $M \subseteq S_\Theta \setminus \{i, j\}$ have been checked.
end for

testing framework to test for invariance between regression coefficients and residual variances. The null hypotheses are

$$H_0^{i,j|S} : \beta_{i,j|S}^{(1)} = \beta_{i,j|S}^{(2)} \quad \text{and} \quad H_0^{j|S} : \sigma_{j|S}^{(1)} = \sigma_{j|S}^{(2)}.$$

We build hypotheses tests based on the F-test. For testing $H_0^{i,j|S}$ we use the test statistic

$$\hat{T} := (\hat{\beta}_{i,j|S}^{(1)} - \hat{\beta}_{i,j|S}^{(2)})^2 \cdot \left[((\hat{\sigma}_{j|M}^{(1)})^2 (n_1 \hat{\Sigma}_{M,M}^{(1)})^{-1} + (\hat{\sigma}_{j|M}^{(2)})^2 (n_2 \hat{\Sigma}_{M,M}^{(2)})^{-1})^{-1} \right]_{i_M i_M}$$

where $\hat{\beta}_{i,j|S}^{(k)}$ is the empirical estimate of $\beta_{i,j|S}^{(k)}$ obtained by ordinary least squares, $(\hat{\sigma}_{j|M}^{(k)})^2$ is an unbiased estimator of the regression residual variance $(\sigma_{j|M}^{(k)})^2$, $\hat{\Sigma}_{M,M}^{(k)}$ is the sample covariance matrix of the random vector $X_M^{(k)}$ with $M = \{i\} \cup S$, and i_M denotes the index in M corresponding to the element i . Lütkepohl (2005)[Section 3.6] shows that under the null hypothesis the asymptotic distribution of \hat{T} can be approximated by the F-distribution $F(1, n_1 + n_2 - 2|S| - 2)$. Similarly, for testing $H_0^{j|S}$, we use the test statistic

$$\hat{F} := (\hat{\sigma}_{j|M}^{(1)})^2 / (\hat{\sigma}_{j|M}^{(2)})^2.$$

Under the null hypothesis, \hat{F} is a ratio of two χ^2 -distributed random variables and hence \hat{F} follows an F-distribution, namely $F(n_1 - |S| - 1, n_2 - |S| - 1)$. See the Supplementary Material for more details regarding these derivations.

Algorithm 3 Directing edges in the difference-DAG

Input: Sample data $\hat{X}^{(1)}$ and $\hat{X}^{(2)}$, estimated set of changed nodes S_Θ , estimated skeleton $\bar{\Delta}$.
Output: Estimated set of arrows \tilde{A}_Δ .
 Set $\tilde{A}_\Delta := \emptyset$;
for each node j incident to at least one undirected edge in $\bar{\Delta}$ **do**
 repeat
 Choose $M \subseteq S_\Theta \setminus \{j\}$,
 if $\sigma_{j|M}^{(k)}$ is invariant across $k = \{1, 2\}$ **then**
 for each undirected edge $i - j$ incident to j in $\bar{\Delta}$ **do**
 Add $i \rightarrow j$ to \tilde{A}_Δ if $i \in M$, otherwise add $j \rightarrow i$ to \tilde{A}_Δ ;
 end for
 end if
 until M is found such that $\sigma_{j|M}^{(k)}$ is invariant or all $M \subseteq S_\Theta \setminus \{j\}$ have been checked.
end for

Example 3.3. We end this section with a 4-node example showing how the DCI algorithm works. Let $B^{(1)}$ and $B^{(2)}$ be the autoregressive matrices defined as shown in Figure 1 and let the error variances satisfy

$$\sigma_1^{(1)} \neq \sigma_1^{(2)}, \sigma_2^{(1)} = \sigma_2^{(2)}, \sigma_3^{(1)} = \sigma_3^{(2)}, \sigma_4^{(1)} \neq \sigma_4^{(2)}.$$

Initiating Algorithm 2 with Δ_Θ being the complete graph and $S_\Theta = [4]$, the DCI output is shown on the right in Figure 1. Note that the edge $1 - 4$ is not oriented, since $\sigma_{4|M}^{(k)}$ and $\sigma_{1|M}^{(k)}$ are not invariant for appropriate $M \subseteq [4]$. However, the edge $1 - 2$ could be oriented in a post-processing step, using the fact that Δ is acyclic. \square

In the final step the PC algorithm orients all edges that are forced by the acyclicity constraint. As explained by Meek (1995), the reason why the PC algorithm can do this efficiently is that it identified all v -structures in the output using CI tests. Unfortunately, as shown in Example 3.3, it is not the case that all v -structures are identifiable just from invari-

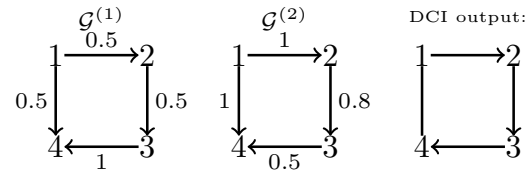


Figure 1. Example of DCI output: The autoregressive matrices $B^{(1)}$ and $B^{(2)}$ are shown as edge weights in $\mathcal{G}^{(1)}$ and $\mathcal{G}^{(2)}$. We assume that the variances of the noise terms $\epsilon_2^{(k)}$ and $\epsilon_3^{(k)}$ are invariant across the two distributions, while the variances of $\epsilon_1^{(k)}$ and $\epsilon_4^{(k)}$ are changed. The DCI output is shown on the right.

ances. In order to orient the edge 1 – 4 in Example 3.3, one would need to identify at least one directed path from 1 to 4, which is computationally intractable in the presence of long directed paths. For small problems one can enumerate all such directed paths to complete the orientations in the DCI output. Such a brute-force algorithm for obtaining more edge orientations is given in the Supplementary Material.

4. Consistency of DCI

Given the discussion above, we say that the DCI algorithm is *consistent* if it outputs a partially oriented graph $\hat{\Delta}$ that has the same skeleton as the true difference-DAG and whose oriented edges are all correctly oriented. Just as methods for estimating a single DAG require assumptions on the underlying model (e.g. the faithfulness assumption) to ensure consistency, our method for estimating the difference-DAG requires assumptions on relationships between the two underlying models.

To define these assumptions it is helpful to view $(\sigma_j^{(k)})_{j \in [p]}$ and the non-zero entries $(B_{ij}^{(k)})_{(i,j) \in A^{(k)}}$ as *variables* or *indeterminates* and each entry of $\Theta^{(k)}$ as a *rational function*, i.e., a fraction of two *polynomials* in the variables $B_{ij}^{(k)}$ and $\sigma_j^{(k)}$ as defined in (1). Using Schur complements one can then similarly express $\beta_{v,w|S}^{(k)}$ and $(\sigma_w^{(k)})^2$ as a rational function in the entries of $\Theta^{(k)}$ and hence as a rational function in the variables $(B_{ij}^{(k)})_{(i,j) \in A^{(k)}}$ and $(\sigma_j^{(k)})_{j \in [p]}$. The exact formulae are given in the Supplementary Material.

Now it is obvious that if

$$B_{ij}^{(1)} = B_{ij}^{(2)} \quad \forall (i, j) \quad \text{and} \quad \sigma_j^{(1)} = \sigma_j^{(2)} \quad \forall j \in [p],$$

then $\beta_{v,w|S}^{(1)} = \beta_{v,w|S}^{(2)}$ and $\sigma_w^{(1)} = \sigma_w^{(2)}$ for all v, w, S . In the DCI algorithm we assume that the converse is true as well, namely that *differences* in B_{ij} and σ_j in the two distributions are not “cancelled out” by changes in other variables and result in differences in the regression coefficients and regression residual variances. This allows us to deduce invariance patterns of the autoregressive matrix $B^{(k)}$ from invariance patterns of the regression coefficients and regression residual variances, and hence differences of the two causal DAGs.¹ To formalize these assumptions, note that if $B_{ij}^{(k)} \neq 0$, then $B_{ij}^{(k)}$ appears as a variable in the rational functions of $\beta_{i,j|S}^{(k)}$, $\beta_{j,i|S}^{(k)}$, $(\sigma_j^{(k)})^2$ and $(\sigma_{i|S \cup \{j\}}^{(k)})^2$ for all $S \subseteq [p] \setminus \{i, j\}$. Similarly, $\sigma_j^{(k)}$ is a variable in the

¹This is similar to the faithfulness assumption in the Gaussian setting, where partial correlations are used for CI testing; the partial correlations are rational functions in the variables $B_{ij}^{(k)}$ and $\sigma_j^{(k)}$ and the faithfulness assumption asserts that if a partial correlation $\rho_{ij|S}$ is zero then the corresponding rational function is identically equal to zero and hence $B_{ij} = 0$ (Lin et al., 2014).

rational function of $(\sigma_j^{(k)})^2$ for all $S \subseteq [p] \setminus \{j\}$. Hence it is sufficient to consider the rational functions given by the regression coefficients and regression residual variances and we obtain the following assumptions.

Assumption 4.1 (Difference-adjacency-faithfulness assumption). *For any choices of $i, j \in S_\Theta$, if $B_{ij}^{(1)} \neq B_{ij}^{(2)}$, then for all $S \subseteq S_\Theta \setminus \{i, j\}$ it holds that*

$$\beta_{i,j|S}^{(1)} \neq \beta_{i,j|S}^{(2)} \quad \text{and} \quad \beta_{j,i|S}^{(1)} \neq \beta_{j,i|S}^{(2)}.$$

Assumption 4.2 (Difference-orientation-faithfulness assumption). *For any choices of $i, j \in S_\Theta$ it holds that*

1. *if $B_{ij}^{(1)} \neq B_{ij}^{(2)}$, then $\forall S \subseteq S_\Theta \setminus \{i, j\}$:*

$$\sigma_{j|S}^{(1)} \neq \sigma_{j|S}^{(2)} \quad \text{and} \quad \sigma_{i|S \cup \{j\}}^{(1)} \neq \sigma_{i|S \cup \{j\}}^{(2)}.$$

2. *if $\sigma_j^{(1)} \neq \sigma_j^{(2)}$, then $\sigma_{j|S}^{(1)} \neq \sigma_{j|S}^{(2)}$ for all $S \subseteq S_\Theta \setminus \{j\}$.*

Assumption 4.1 ensures that the skeleton of the difference-DAG is inferred correctly, whereas Assumption 4.2 ensures that the arrows returned by DCI are oriented correctly. These assumptions are the equivalent of the *adjacency-faithfulness* and *orientation-faithfulness* assumptions that ensure consistency of the PC algorithm for estimating the MEC of a causal DAG (Ramsey et al., 2006). For example, the adjacency-faithfulness assumption (in the Gaussian setting) asserts that if $B_{ij} \neq 0$ then for all $S \subseteq [p] \setminus \{i, j\}$ the partial correlations $\rho_{ij|S} \neq 0$. While the adjacency-faithfulness assumption is concerned with the non-zero pattern of B and the non-zero pattern of the partial correlations, Assumption 4.1 is concerned with the non-zero pattern of the *differences* $B^{(1)} - B^{(2)}$ and the non-zero pattern of the *differences* in regression coefficients $\beta_{i,j|S}^{(1)} - \beta_{i,j|S}^{(2)}$.

We now provide the main results of this paper, namely regarding consistency of the DCI algorithm. For simplicity we here provide the consistency guarantees when Algorithm 2 is initialized with Δ_Θ being the complete graph and $S_\Theta = [p]$. The disadvantage of such an initialization as compared to using the difference-UG is that the number of hypothesis tests needed in the DCI algorithm is in general larger. However, DCI is consistent, as long as it is initialized using an algorithm that is consistent for estimating the difference-UG (see proofs in the Supplementary Material). This is the case for example for KLIEP in the Gaussian noise setting. For general additive noise models we provide a constraint-based algorithm for learning the difference-UG with consistency guarantees in the Supplementary Material.

Theorem 4.3. *Given Assumption 4.1, Algorithm 2 is consistent in estimating the skeleton of the difference-DAG Δ .*

The proof is given in the Supplementary Material. The main ingredient of the proof is to show that if $B_{ij}^{(1)} = B_{ij}^{(2)}$, then

there exists a conditioning set $S \subseteq S_\Theta \setminus \{i, j\}$ such that $\beta_{i,j|S}^{(1)} = \beta_{i,j|S}^{(2)}$. When the DCI algorithm is initialized with $S_\Theta = [p]$, then letting S consist of the union of parents of node j in both DAGs excluding node i results in $\beta_{i,j|S}^{(k)} = B_{ij}^{(k)}$. In the Supplementary Material we prove that when initialized in the difference-UG, by interpreting $\beta_{i,j|S}^{(k)}$ as a rational function of the variables in the d-connecting paths that connect i and j given S , a suitable S still exists. Next, we provide consistency guarantees for Algorithm 3.

Theorem 4.4. *Given Assumption 4.2, all arrows \tilde{A}_Δ output by Algorithm 3 are correctly oriented. In addition, $i \rightarrow j \in \tilde{A}_\Delta$ if and only if the variance of either $\epsilon_i^{(k)}$ or $\epsilon_j^{(k)}$ is invariant across $k = \{1, 2\}$.*

Similarly as the proof of Theorem 4.3, the proof follows by interpreting the rational functions corresponding to regression residual variances in terms of d-connecting paths and is given in the Supplementary Material. It is important to note that as a direct corollary to Theorem 4.4 we obtain sufficient conditions for full identifiability of the difference-DAG (i.e., all arrows) using the DCI algorithm.

Corollary 4.5. *Given Assumptions 4.1 and 4.2, and assuming that the error variances are the same across the two distributions, i.e. $\Omega^{(1)} = \Omega^{(2)}$, the DCI algorithm outputs the difference-DAG Δ .*

We end this section with two remarks, namely regarding the sample complexity of the DCI algorithm and an evaluation of how restrictive Assumptions 4.1 and 4.2 are.

Remark 4.6 (Sample complexity of DCI in the high-dimensional setting). *Kalisch & Bühlmann (2007) showed that for constraint-based methods such as the PC or DCI algorithms, the sample complexity is determined by the number of hypothesis tests performed by the algorithm. In the high-dimensional setting, the number of hypothesis tests performed by the PC algorithm scales as $\mathcal{O}(p^s)$, where p is the number of nodes and s is the maximum degree of the DAG, thereby implying severe restrictions on the sparsity of the DAG given a reasonable sample size. Meanwhile, the number of hypothesis tests performed by the DCI algorithm scales as $\mathcal{O}(|\Delta_\Theta|2^{|\mathcal{S}_\Theta|-1})$ and hence does not depend on the degree of the two DAGs. Therefore, even if the two DAGs $\mathcal{G}^{(1)}$ and $\mathcal{G}^{(2)}$ are high-dimensional and highly connected, the DCI algorithm is consistent and has a better sample complexity (as compared to estimating two DAGs separately) as long as the differences between $\mathcal{G}^{(1)}$ and $\mathcal{G}^{(2)}$ are sparse, i.e., $|\mathcal{S}_\Theta|$ is small compared to p and s .* \square

Remark 4.7 (Strength of Assumptions 4.1 and 4.2). *Since it was shown that the faithfulness assumption, a standard assumption for consistency of causal inference algorithms to estimate an MEC, is very restrictive, it is of interest to compare Assumptions 4.1 and 4.2 to the faithfulness assumption of $\mathbb{P}^{(k)}$ with respect to $\mathcal{G}^{(k)}$ for $k \in \{1, 2\}$. In the*

Supplementary Material we provide examples showing that Assumptions 4.1 and 4.2 do not imply the faithfulness assumption on the two distributions and vice-versa. However, following the analysis of the faithfulness assumption in Uhler et al. (2013), we expect Assumptions 4.1 and 4.2 to be weaker than the faithfulness assumption in the finite sample regime. The reason is that violations of the faithfulness assumption as well as of Assumptions 4.1 and 4.2 correspond to hypersurfaces in the variables B_{ij} and σ_j . The number of these hypersurfaces is increasing in s for the faithfulness assumption and in S_Θ for Assumptions 4.1 and 4.2. Hence if the two DAGs $\mathcal{G}^{(1)}$ and $\mathcal{G}^{(2)}$ are large and contain hub nodes, while their difference is sparse, then $S_\Theta \ll s$ and the volume of points that are close to these hypersurfaces (i.e., corresponding to violations of the assumptions in the finite-sample regime) is smaller for Assumptions 4.1 and 4.2 as compared to the faithfulness assumption. \square

5. Evaluation

In this section we evaluate our method based on synthetic data and two gene expression data sets.

5.1. Synthetic data

We analyzed the performance of our algorithm in both, the low- and high-dimensional setting. For both settings we generated 100 realizations of pairs of upper-triangular SEMs $(B^{(1)}, \epsilon^{(1)})$ and $(B^{(2)}, \epsilon^{(2)})$. For $B^{(1)}$, the graphical structure was generated using an Erdős-Renyi model with expected neighbourhood size s , on p nodes and n samples. The edge weights were uniformly drawn from $[-1, -0.25] \cup [0.25, 1]$ to ensure that they were bounded away from zero. $B^{(2)}$ was then generated from $B^{(1)}$ by adding and removing edges with probability 0.1, i.e.,

$$B_{ij}^{(2)} \stackrel{\text{i.i.d.}}{\sim} \text{Ber}(0.9) \cdot B_{ij}^{(1)} \text{ if } B_{ij}^{(1)} \neq 0$$

$$B_{ij}^{(2)} \stackrel{\text{i.i.d.}}{\sim} \text{Ber}(0.1) \cdot \text{Unif}([-1, -0.25] \cup [0.25, 1]) \text{ if } B_{ij}^{(1)} = 0$$

Note that while the DCI algorithm is able to identify changes in edge weights, we only generated DAG models that differ by edge insertions and deletions. This is to provide a fair comparison to the naive approach, where we separately estimate the two DAGs $\mathcal{G}^{(1)}$ and $\mathcal{G}^{(2)}$ and then take their difference, since this approach can only identify insertions and deletions of edges.

In Figure 2 we analyzed the performance of the DCI algorithm in the low-dimensional setting. The simulations were performed on graphs with $p = 10$ nodes, neighborhood size of $s = 3$ and sample size $n \in \{10^3, 10^4\}$. For Figure 2 (a) and (b) we set $\epsilon^{(1)}, \epsilon^{(2)} \sim \mathcal{N}(0, \mathbf{1}_p)$, which by Corollary 4.5 ensures that the difference-DAG Δ is fully identifiable. We compared the performance of DCI to the naive approach, where we separately estimated the two DAGs $\mathcal{G}^{(1)}$ and $\mathcal{G}^{(2)}$

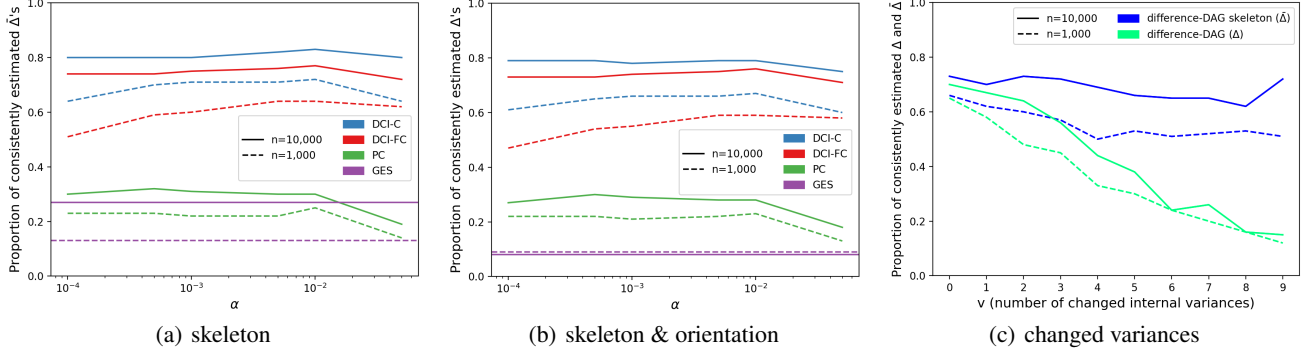


Figure 2. The proportion of consistently estimated difference-DAGs for 100 realizations per setting with $p = 10$ nodes and sample size n . Figures (a) and (b) show the proportion of consistently estimated difference-DAGs when considering just the skeleton ($\bar{\Delta}$) and when considering both skeleton and edge orientations (Δ) respectively; α is the significance level used for the hypothesis tests in the algorithms. Figure (c) shows the proportion of consistent estimates with respect to the number of changes in internal node variances v .

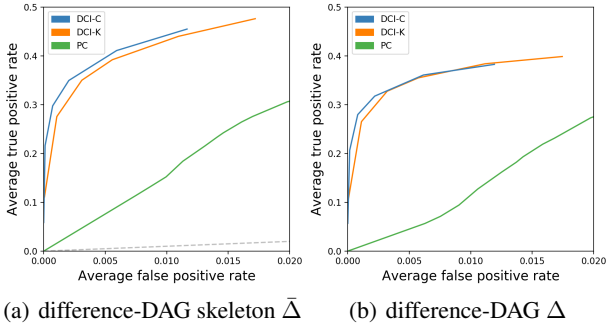


Figure 3. ROC curves for estimating the difference-DAG Δ and its skeleton $\bar{\Delta}$ with $p = 100$ nodes, expected neighbourhood size $s = 10$, $n = 300$ samples, and 5% change between DAGs.

and then took their difference. For the separate estimation we used the prominent PC and GES algorithms. For the DCI algorithm we analyzed two different initializations, namely using Δ_{Θ} being the fully connected graph and $S_{\Theta} = [p]$ (DCI-FC) and using the constraint-based method described in the Supplementary Material to estimate the difference-UG (DCI-C). Both initializations provide a provably consistent algorithm. Figure 2 (a) and (b) show the proportion of consistently estimated difference-DAGs either by just considering the skeleton ($\bar{\Delta}$), or considering both skeleton and orientations (Δ). For PC and GES, we considered the set of edges that appear in one estimated skeleton but disappear in another as the estimated skeleton of the difference-DAG $\bar{\Delta}$. In determining orientations, we considered the arrows that were directed in one estimated CP-DAG but disappeared in another as the estimated set of directed arrows. Since the main purpose of this low-dimensional simulation study is to validate our theoretical findings, we used the exact recovery rate as evaluation criterion. In line with our theoretical findings, both variants of the DCI algorithm outperformed taking differences after separate estimation for learning the difference-DAG. Figure 2 (a) and (b) also show that the PC algorithm outperformed GES in estimating the difference-

DAG, which is unexpected given previous results showing that GES usually has a higher exact recovery rate than the PC algorithm when estimating a single DAG. This is due to the fact that while the PC algorithm usually estimates less DAGs correctly, the incorrectly estimated DAGs tend to look more similar to the true model than the incorrect estimates of GES (as also reported by Solus et al. (2017)) and can still lead to a correct estimate of the difference-DAG.

In Figure 2 (c) we analyzed the effect of changes in the noise variances on estimation performance and set $\epsilon^{(1)} \sim \mathcal{N}(0, \mathbf{1}_p)$, while for $\epsilon^{(2)}$, we randomly picked v nodes and uniformly sampled their variances from $[1.25, 2]$. We used $\alpha = .05$ as significance level based on the evaluation from Figure 2 (a) and (b). Figure 2 (c) shows that in line with Theorem 4.4, as we increase the number of nodes i such that $\epsilon_i^{(1)} \neq \epsilon_i^{(2)}$, the number of edges whose orientations can be determined decreases. This is because Algorithm 3 can only determine an edge's orientation when the variance of at least one of its nodes is invariant. Moreover, Figure 2 (c) shows that the accuracy of Algorithm 2 is not impacted by changes in the noise variances.

Finally, Figure 3 shows the performance of the DCI algorithm in the high-dimensional setting. The simulations were performed on graphs with $p = 100$ nodes, expected neighborhood size of $s = 10$ and sample size $n = 300$. $B^{(2)}$ was derived from $B^{(1)}$ so that the total number of changes was 5% of the total number of edges in $B^{(1)}$, with an equal amount of insertions and deletions. We generated $\epsilon^{(1)}, \epsilon^{(2)} \sim \mathcal{N}(0, \mathbf{1}_p)$. Figure 3 shows the ROC curves for estimating the difference-DAG and its skeleton. Since the PC algorithm outperformed GES in the low-dimensional setting, we here omitted the results for GES. Similarly, we omitted DCI-FC. In addition, we also considered using KLIEP for initializing the DCI algorithm (DCI-K). Figure 3 shows that both DCI-FC and DCI-K perform similarly well and outperform separate estimation using the PC algorithm. The results for 10% change is in the Supplementary Material.

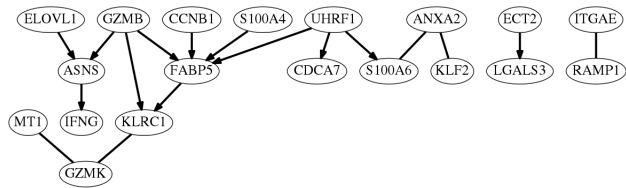


Figure 4. Estimate of the difference-DAG model between gene expression data from naive and activated T cells.

5.2. Real data analysis

Ovarian cancer. We tested our method on an ovarian cancer data set (Tothill et al., 2008) that contains two groups of patients with different survival rates and was previously analyzed using the DPM algorithm for learning the difference-UG (Zhao et al., 2014). We followed the analysis of Zhao et al. (2014) and applied the DCI algorithm to gene expression data from the apoptosis and TGF- β pathways. In the apoptosis pathway, we identified two hub nodes: BIRC3 and PRKAR2B. BIRC3, also discovered by DPM, has been shown to be an inhibitor of apoptosis (Johnstone et al., 2008) and is one of the main deregulated genes in ovarian cancer (Jönsson et al., 2014). PRKAR2B, not identified by DPM, has been shown to be important in disease progression in ovarian cancer cells (Cheadle et al., 2008) and an important regulatory unit for cancer cell growth (Chiaradonna et al., 2008). In addition, the RII- β protein encoded by PRKAR2B has been considered as a therapeutic target for cancer therapy (Mikalsen et al., 2006; Cho-Chung, 1999), thereby confirming the relevance of our findings. With respect to the TGF- β pathway, the DCI method identified THBS2 and COMP as hub nodes. Both of these genes have been implicated in resistance to chemotherapy in epithelial ovarian cancer (Marchini et al., 2013) and were also recovered by DPM. Overall, the difference-UG discovered by DPM is comparable to the difference-DAG found by our method. For more details regarding this analysis, see the Supplementary Material.

T cell activation. To demonstrate the relevance of our method for current genomics applications, we applied DCI to single-cell gene expression data of naive and activated T cells in order to study the pathways involved during the immune response to a pathogen. We analyzed single-cell gene expression data from 377 activated and 298 naive T cells obtained by Singer et al. (2016) using the recent drop-seq technology. From the previously identified differentially expressed genes between naive and activated T cells (Sarkar et al., 2008), we selected all genes that had a fold expression change above 10, resulting in 60 genes for further analysis.

To initiate DCI, we estimated the difference-UG using KLIEP, thresholding the edge weights at 0.005. We ran DCI for different tuning parameters and with cross-validation to obtain the final DCI output shown in Figure 4 using sta-

bility selection as proposed by (Meinshausen & Bühlmann, 2010). The genes with highest out-degree, and hence of interest for future interventional experiments, are GZMB and UHRF1. Interestingly, GZMB (granzyme B) is known to induce cytotoxicity, which is important during immune response for attacking and killing the invading pathogen. Furthermore, this gene has been found to be expressed in a large fraction of T cells during peak of the exponential T cell growth and it has been reported as the most differentially expressed gene during T cell activation (Peixoto et al., 2007; Hatton, 2013). UHRF1 has been shown to be critical for T cell maturation and proliferation through knockout experiments (Obata et al., 2014; Cui et al., 2016). Interestingly, the UHRF1 protein is a transcription factor, i.e. it binds to DNA sequences and regulates the expression of other genes, thereby confirming its role as an important causal regulator and a suitable interventional candidate. Learning a difference-DAG as opposed to a difference-UG is crucial for prioritizing genes. The difference UG for this application would not only have been more dense, but it would also have resulted in additional hub nodes such as FABP5, KLRC1, and ASNS, which based on the current biological literature seem secondary to T cell activation (FABP5 is involved in lipid binding, KLRC1 has a role in natural killer cells but not in T cells, and ASNS is an asparagine synthetase gene).

6. Discussion

We have presented an algorithm for directly estimating the difference between two causal DAG models given i.i.d. samples from each model. To our knowledge this is the first such algorithm and is of particular interest for learning differences between related networks, where each network might be dense, while the difference is sparse. We provided consistency guarantees for our algorithm and showed on synthetic and real data that it outperforms the naive approach of separately estimating two DAG models and taking their difference. We applied our algorithm to gene expression data in bulk and from single cells, showing that DCI is able to identify biologically relevant genes for ovarian cancer and T-cell activation. This purports DCI as a promising method for identifying intervention targets that are causal for a particular phenotype for subsequent experimental validation. In order to make DCI scale to networks with thousands of nodes, an important challenge is to reduce the number of hypothesis tests. The PC algorithm achieves this by dynamically updating the list of CI tests given the current estimate of the graph. It is an open problem whether one can similarly reduce the number of hypothesis tests for DCI. Furthermore, in many applications (e.g., when comparing normal to disease states), there is an imbalance of data/prior knowledge for the two models. In future work it would be interesting to develop methods that can make use of this to directly learn the differences between the two models.

References

- Andersson, S. A., Madigan, D., and Perlman, M. D. A characterization of markov equivalence classes for acyclic digraphs. *The Annals of Statistics*, 25(2):505–541, 1997.
- Barabási, A.-L. and Oltvai, Z. N. Network biology: understanding the cell’s functional organization. *Nature Reviews Genetics*, 5(2):101–113, 2004.
- Barabási, A.-L., Gulbahce, N., and Loscalzo, J. Network medicine: a network-based approach to human disease. *Nature Reviews Genetics*, 12(1):56–68, 2011.
- Cheadle, C., Nesterova, M., Watkins, T., Barnes, K. C., Hall, J. C., Rosen, A., Becker, K. G., and Cho-Chung, Y. S. Regulatory subunits of PKA define an axis of cellular proliferation/differentiation in ovarian cancer cells. *BMC Medical Genomics*, 1(1):43, 2008.
- Chiaradonna, F., Balestrieri, C., Gaglio, D., and Vanoni, M. RAS and PKA pathways in cancer: new insight from transcriptional analysis. *Frontiers in Bioscience*, 13:5257–5278, 2008.
- Cho-Chung, Y. S. Antisense oligonucleotide inhibition of serine/threonine kinases: an innovative approach to cancer treatment. *Pharmacology & Therapeutics*, 82(2):437–449, 1999.
- Cui, Y., Chen, X., Zhang, J., Sun, X., Liu, H., Bai, L., Xu, C., and Liu, X. Uhrf1 Controls iNKT Cell Survival and Differentiation through the Akt-mTOR Axis. *Cell Reports*, 15(2):256–263, 2016.
- Draisma, J., Sullivant, S., and Talaska, K. Positivity for gaussian graphical models. *Advances in Applied Mathematics*, 50(5):661–674, 2013.
- Drton, M. and Perlman, M. D. Multiple testing and error control in gaussian graphical model selection. *Statistical Science*, pp. 430–449, 2007.
- Friedman, N., Linal, M., Nachman, I., and Pe’er, D. Using bayesian networks to analyze expression data. *Journal of Computational Biology*, 7(3-4):601–620, 2000.
- Hatton, L. A. *Molecular mechanisms regulating CD8+ T cell granzyme and perforin gene expression*. PhD thesis, University of Melbourne, 2013.
- Hudson, N. J., Reverter, A., and Dalrymple, B. P. A differential wiring analysis of expression data correctly identifies the gene containing the causal mutation. *PLoS Computational Biology*, 5(5):e1000382, 2009.
- Johnstone, R.W., Frew, A.J., and Smyth, M.J. The TRAIL apoptotic pathway in cancer onset, progression and therapy. *Nature Reviews Cancer*, 8(10):782–798, 2008.
- Jönsson, J., Bartuma, K., Dominguez-Valentin, M., Harbst, K., Ketabi, Z., Malander, S., Jönsson, M., Carneiro, A., Måsbäck, A., Jönsson, G., and Nilbert, M. Distinct gene expression profiles in ovarian cancer linked to Lynch syndrome. *Familial Cancer*, 13:537–545, 2014.
- Kalisch, M. and Bühlmann, P. Estimating high-dimensional directed acyclic graphs with the pc-algorithm. *Journal of Machine Learning Research*, 8(Mar):613–636, 2007.
- Kanehisa, M., Goto, S., Sato, Y., Furumichi, M., and Mao, T. KEGG for integration and interpretation of large-scale molecular data sets. *Nucleic Acids Research*, 40(D1):D109–D114, 2011.
- Lauritzen, S. L. *Graphical models*, volume 17. Clarendon Press, 1996.
- Lin, S., Uhler, C., Sturmfels, B., and Bühlmann, P. Hypersurfaces and their singularities in partial correlation testing. *Foundations of Computational Mathematics*, 14(5):1079–1116, 2014.
- Liu, S., Quinn, J. A., Gutmann, M. U., Suzuki, T., and Sugiyama, M. Direct learning of sparse changes in markov networks by density ratio estimation. *Neural Computation*, 26(6):1169–1197, 2014.
- Liu, S., Fukumizu, K., and Suzuki, T. Learning sparse structural changes in high-dimensional markov networks. *Behaviormetrika*, 44(1):265–286, 2017.
- Lütkepohl, Helmut. *New introduction to multiple time series analysis*. Springer Science & Business Media, 2005.
- Marchini, S., Fruscio, R., Clivio, L., Beltrame, L., Porcu, L., Nerini, I. F., Cavalieri, D., Chiorino, G., Cattoretti, G., Mangioni, C., Milani, R., Torri, V., Romualdi, C., Zambelli, A., Romano, M., Signorelli, M., di Giandomenico, S., and D’Incalci, M. Resistance to platinum-based chemotherapy is associated with epithelial to mesenchymal transition in epithelial ovarian cancer. *European Journal of Cancer*, 49(2):520–530, 2013.
- Meek, C. Causal inference and causal explanation with background knowledge. In *Proceedings of the Eleventh conference on Uncertainty in artificial intelligence*, pp. 403–410. Morgan Kaufmann Publishers Inc., 1995.
- Meek, C. *Graphical Models: Selecting causal and statistical models*. PhD thesis, Carnegie Mellon University, 1997.
- Meinshausen, N. and Bühlmann, P. Stability selection. *Journal of the Royal Statistical Society. Series B: Statistical Methodology*, 72(4):417–473, 2010.

- Mikalsen, T., Gerits, N., and Moens, U. Inhibitors of signal transduction protein kinases as targets for cancer therapy. *Biotechnology Annual Review*, 12:153–223, 2006.
- Nandy, P., Hauser, A., and Maathuis, M. H. High-dimensional consistency in score-based and hybrid structure learning. *arXiv preprint arXiv:1507.02608*, 2015.
- Obata, Y., Furusawa, Y., Endo, T.A., Sharif, J., Takahashi, D., Atarashi, K., Nakayama, M., Onawa, S., Fujimura, Y., Takahashi, M., Ikawa, T., Otsubo, T., Kawamura, Y.I., Dohi, T., Tajima, S., Masumoto, H., Ohara, O., Honda, K., Hori, S., Ohno, H., Koseki, H., and Hase, K. The epigenetic regulator Uhrf1 facilitates the proliferation and maturation of colonic regulatory T cells. *Nature Immunology*, 15(6):571–579, 2014.
- Ogata, H., Goto, S., Sato, K., Fujibuchi, W., Bono, H., and Kanehisa, M. KEGG: Kyoto encyclopedia of genes and genomes. *Nucleic Acids Research*, 27(1):29–34, 1999.
- Pearl, J. *Causality: Models, Reasoning, and Inference*. Cambridge University Press, 2000.
- Peixoto, A., Evaristo, C., Munitic, I., Monteiro, M., Charbit, A., Rocha, B., and Veiga-Fernandes, H. CD8 single-cell gene coexpression reveals three different effector types present at distinct phases of the immune response. *The Journal of Experimental Medicine*, 204(5):1193–1205, 2007.
- Pimanda, J. E., Ottersbach, K., Knezevic, K., Kinston, S., Chan, W. Y., Wilson, N. K., Landry, J., Wood, A. D., Kolb-Kokocinski, A., Green, A. R., Tannahill, D., Lacaud, G., Kouskoff, V., and Göttgens, B. Gata2, Fli1, and Scl form a recursively wired gene-regulatory circuit during early hematopoietic development. *Proceedings of the National Academy of Sciences*, 104(45):17692–17697, 2007.
- Pourahmadi, M. Covariance estimation: The glm and regularization perspectives. *Statistical Science*, pp. 369–387, 2011.
- Ramsey, J., Spirtes, P., and Zhang, J. Adjacency-faithfulness and conservative causal inference. In *Proceedings of the Twenty-Second Conference on Uncertainty in Artificial Intelligence*, pp. 401–408. AUAI Press, 2006.
- Robins, J. M. and Hernan, Miguel. A. and Brumback, B. Marginal structural models and causal inference in epidemiology, 2000.
- Sanei, S. and Chambers, J. A. *EEG Signal Processing*. John Wiley & Sons, 2013.
- Sarkar, S., Kalia, V., Haining, W.N., Konieczny, B.T., Subramaniam, S., and Ahmed, R. Functional and genomic profiling of effector CD8 T cell subsets with distinct memory fates. *The Journal of Experimental Medicine*, 205(3): 625–640, 2008.
- Singer, M., Wang, C., Cong, L., Marjanovic, N.D., Kowalczyk, M.S., Zhang, H., Nyman, J., Sakuishi, K., Kurtulus, S., Gennert, D., Xia, J., Kwon, J.Y.H., Nevin, J., Herbst, R.H., Yanai, I., Rozenblatt-Rosen, O., Kuchroo, V.K., Regev, A., and Anderson, A.C. A Distinct Gene Module for Dysfunction Uncoupled from Activation in Tumor-Infiltrating T Cells. *Cell*, 166(6):1500–1511, 2016.
- Solus, L., Wang, Y., Matejovicova, L., and Uhler, C. Consistency guarantees for permutation-based causal inference algorithms. *arXiv preprint arXiv:1702.03530*, 2017.
- Spirtes, P., Glymour, C. N., and Scheines, R. *Causation, prediction, and search*. MIT press, 2000.
- Tohill, R. W., Tinker, A. V., George, J., Brown, R., Fox, S. B., Lade, S., Johnson, D. S., Trivett, M. K., Etemadmoghadam, D., Locandro, B., Traficante, N., Fereday, S., Hung, J. A., Chiew, Y., Haviv, I., Group, Australian Ovarian Cancer Study, Gertig, D., deFazio, A., and Bowtell, D. D.L. Novel molecular subtypes of serous and endometrioid ovarian cancer linked to clinical outcome. *Clinical Cancer Research*, 14(16):5198–5208, 2008.
- Tsamardinos, I., Brown, L. E., and Aliferis, C. F. The maximum hill-climbing bayesian network structure learning algorithm. *Machine Learning*, 65(1):31–78, 2006.
- Uhler, C., Raskutti, G., Bühlmann, P., and Yu, B. Geometry of the faithfulness assumption in causal inference. *The Annals of Statistics*, pp. 436–463, 2013.
- Van de Geer, S. and Bühlmann, P. ℓ_0 -penalized maximum likelihood for sparse directed acyclic graphs. *The Annals of Statistics*, 41(2):536–567, 2013.
- Verma, T. and Pearl, J. Equivalence and synthesis of causal models. In *Proceedings of the Sixth Annual Conference on Uncertainty in Artificial Intelligence*, pp. 255–270. Elsevier Science Inc., 1990.
- Zhao, S. D., Cai, T. T., and Li, H. Direct estimation of differential networks. *Biometrika*, 101(2):253–268, 2014.

A. Analysis of hypothesis test $H_0^{i,j|S}$

In this section, we explain our use of an F-test on the statistic \hat{T} for the null hypothesis $H_0^{i,j|S}$. For $M := S \cup \{i\}$, let $\beta_M^{(k)}$ be the best linear predictor when regressing $X_j^{(k)}$ onto $X_M^{(k)}$, i.e., our estimator is $X_j^{(k)} = (\beta_M^{(k)})^T X_M^{(k)} + \tilde{\epsilon}_j^{(k)}$. Let β be the vector

$$\beta := \begin{bmatrix} \beta_M^{(1)} \\ \beta_M^{(2)} \end{bmatrix},$$

and let $C \in \mathbb{R}^{2|M|}$ have $C_{i_M} = 1$ and $C_{|M|+i_M} = -1$ and all other entries as zero. Then the null hypothesis $H_0^{i,j|S}$ can be written as: $C^T \beta = 0$. It follows from Proposition 3.5 of (Lütkepohl, 2005), on the asymptotic distribution of the Wald statistic, that \hat{T} converges in distribution to $\chi^2(1)$, i.e., a χ^2 -distribution with 1 degree of freedom.

However, the F-distribution $F(1, n_1 + n_2 - 2|S| - 2)$ is a better approximation for the distribution of \hat{T} , as outlined in Section 3.6 of (Lütkepohl, 2005). A brief justification is in order. First, we know that the convergence is the same: for an F-distribution $F(1, d)$, as $d \rightarrow \infty$, we have $F(1, d) \xrightarrow{d} \chi^2(1)$. Additionally, $F(1, d)$ and \hat{T} both have a fatter tail than $\chi^2(1)$. Together, these facts suggest the choice of a F-distribution $F(1, d)$ with $d \rightarrow \infty$ as $n_1, n_2 \rightarrow \infty$. For the second parameter d , we choose $d = n_1 + n_2 - 2|S| - 2$, the total degrees of freedom of the unbiased estimators of the two regression residual variances, i.e., $(\hat{\sigma}_{j|M}^{(1)})^2$ and $(\hat{\sigma}_{j|M}^{(2)})^2$.

B. A brute-force algorithm for orienting edges

Algorithm B.1 is an alternative to Algorithm 3 for orienting edges. In some cases, Algorithm B.1 can determine more orientations than Algorithm 3 by ensuring the acyclicity constraint is not violated. However, this requires enumerating all possible chains, which could be very time consuming and is therefore not applicable for our problem.

C. Theoretical analysis

C.1. Preliminaries: Schur complement

In this section, we give the exact formula of the Schur complement, and describe how to use the Schur complement to express $\beta_{i,j|S}^{(k)}$ and $(\sigma_{j|S}^{(k)})^2$. This will be used for the proofs of Theorems 4.3 and 4.4 in the following sections.

For a subset of nodes $M \subseteq [p]$, let X_M denote the random vector spanned by the random variables X_i for all $i \in M$. Let $\neg M$ denote the complement of M with respect to the full set of nodes, i.e., $\neg M := [p] \setminus M$. The inverse covariance matrix of the random vector X_M , i.e., $(\Sigma_{M,M})^{-1}$, can

Algorithm B.1 Directing edges in the difference-DAG (Brute force)

Input: Sample data $\hat{X}^{(1)}$ and $\hat{X}^{(2)}$, estimated set of changed nodes S_Θ , estimated skeleton $\bar{\Delta}$.

Output: Estimated set of arrows \hat{A}_Δ .

Set $\hat{A}_\Delta := \emptyset$;

for each node j incident to at least one undirected edge in $\bar{\Delta}$ **do**

repeat

 Choose $M \subseteq S_\Theta \setminus \{j\}$,

if $\sigma_{j|M}^{(k)}$ is invariant across $k = \{1, 2\}$ **then**

for each undirected edge $i - j$ incident to j in $\bar{\Delta}$ **do**

 Add $i \rightarrow j$ to \hat{A}_Δ if $i \in M$, otherwise add $j \rightarrow i$;

end for

end if

until M is found such that $\sigma_{j|M}^{(k)}$ is invariant or all $M \subseteq S_\Theta \setminus \{j\}$ have been checked.

end for

Try to orient as many undirected edges as possible by the following rule:

Orient $i - j$ into $i \rightarrow j$ whenever there is a chain $i \rightarrow \ell_1 \rightarrow \dots \rightarrow \ell_t \rightarrow j$.

be obtained from Θ by taking the Schur complement:

$$\begin{aligned} \Theta_M &:= (\Sigma_{M,M})^{-1} \\ &= \Theta_{M,M} - \Theta_{M,\neg M}(\Theta_{\neg M,\neg M})^{-1}\Theta_{\neg M,M}. \end{aligned}$$

Note that here Θ_M does not represent the submatrix of Θ with set of row and column indices in M , i.e., $\Theta_{M,M}$, but rather the Schur complement. For any two indices $i, j \in M$, let $i_M, j_M \in [|M|]$ denote the row/column indices of matrix Θ_M associated to i and j , then the (i_M, j_M) -th entry of matrix Θ_M can be written as:

$$(\Theta_M)_{i_M j_M} = \Theta_{ij} - \Theta_{i,\neg M}(\Theta_{\neg M,\neg M})^{-1}\Theta_{\neg M,j}.$$

Lin et al. (2014), Draisma et al. (2013) and Uhler et al. (2013) also give a combinatorial characterization of the Schur complement. Following their characterization, the value of $(\Theta_M)_{i_M j_M}$ is determined by the parameters of the d -connecting paths from node i to j given $M \setminus \{i, j\}$. In this case, the entry $(\Theta_M^{(k)})_{i_M j_M}$ would be invariant for $k = \{1, 2\}$ if the parameters along the d -connecting paths are all the same. Finally, by applying the result of (Pourahmadi,

2011), $\beta_{i,j|S}^{(k)}$ and $(\sigma_{j|S}^{(k)})^2$ can be written as:

$$\begin{aligned} \beta_{i,j|S}^{(k)} &= -\frac{(\Theta_M^{(k)})_{i_M j_M}}{(\Theta_M^{(k)})_{j_M j_M}} \quad \text{where } M = S \cup \{i, j\}, \\ (\sigma_{j|S}^{(k)})^2 &= \left((\Theta_M^{(k)})_{j_M j_M} \right)^{-1} \quad \text{where } M = S \cup \{j\}. \end{aligned} \quad (\text{S.2})$$

Combining Eq. (S.2) with the formula for the Schur complement, one can easily see that $\beta_{i,j|S}^{(k)}$ and $(\sigma_{j|S}^{(k)})^2$ can be expressed as rational functions in the variables $(B_{ij}^{(k)})_{(i,j) \in A^{(k)}}$ and $(\sigma_j^{(k)})_{j \in [p]}$.

C.2. Proof of Theorem 4.3

In this Section we provide the consistency proofs of Theorem 4.3 when Algorithm 2 is initialized with difference-UG. The proof of Theorem 4.3 when Algorithm 2 is initialized with the complete graph follows easily from the proofs in this section. To complete the proof, one also needs the following assumption:

Assumption C.1 (Difference-precision-matrix-faithfulness assumption). *For any choices of $i, j \in [p]$, it holds that*

1. If $B_{ij}^{(1)} \neq B_{ij}^{(2)}$, then $\Theta_{ij}^{(1)} \neq \Theta_{ij}^{(2)}$, and for any ℓ with directed path $i \rightarrow j \leftarrow \ell$ in either $\mathcal{G}^{(1)}$ or $\mathcal{G}^{(2)}$, $\ell \in S_\Theta$.
2. If $\sigma_j^{(1)} \neq \sigma_j^{(2)}$, then $\Theta_{jj}^{(1)} \neq \Theta_{jj}^{(2)}$, and $\forall i \in \text{Pa}^{(1)}(j) \cup \text{Pa}^{(2)}(j)$, $i \in S_\Theta$.

Note that Assumption C.1 is not a necessary assumption for the consistency of Algorithm 2, since one can simply take Δ_Θ as the fully connected graph on p nodes and $S_\Theta = [p]$ as input. The same holds for the proof of Theorem 4.4. The strength of Assumption C.1 is further analyzed in Remark C.5.

To prove Theorem 4.3, we need to make use of the following two lemmas:

Lemma C.2. *Given $\Theta^{(1)}$ and $\Theta^{(2)}$, if $\Theta_{ij}^{(1)} = \Theta_{ij}^{(2)}$, then $(\Theta_M^{(1)})_{i_M j_M} = (\Theta_M^{(2)})_{i_M j_M}$ for $M = S_\Theta \cup \{i, j\}$.*

Proof. By Schur complement, we have that $(\Theta_M^{(k)})_{i_M j_M} = \Theta_{ij}^{(k)} - \Theta_{i,-M}^{(k)} (\Theta_{-M,-M}^{(k)})^{-1} \Theta_{-M,j}^{(k)}$. By the definition of S_Θ , $\Theta_{M,-M}^{(1)} = \Theta_{M,-M}^{(2)}$ and $\Theta_{-M,-M}^{(1)} = \Theta_{-M,-M}^{(2)}$. \square

Lemma C.3. *Under Assumption C.1, given two linear SEMs $(B^{(1)}, \epsilon^{(1)})$ and $(B^{(2)}, \epsilon^{(2)})$, for the precision matrix $\Theta^{*(k)}$ of the random vector $X_{1:j}^{(k)}$, we have $S_{\Theta^*} \subseteq S_\Theta$.*

Proof. Since $B^{(k)}$ is strictly upper triangular, the marginal distribution of the random vector $X_{1:j}^{(k)}$ follows a new SEM,

$$X_{1:j}^{(k)} = (B_{1:j,1:j}^{(k)})^T X_{1:j}^{(k)} + \epsilon_{1:j}^{(k)},$$

where $B_{1:j,1:j}^{(k)}$ is the submatrix of $B^{(k)}$ with the first j rows and j columns, and $\epsilon_{1:j}^{(k)}$ is the random vector with the first j random variables of $\epsilon^{(k)}$. It can then be shown the (i, ℓ) -th entry of the new precision matrix Θ^* is given by:

$$\Theta_{i\ell}^{*(k)} = -(\sigma_\ell^{(k)})^{-2} B_{i\ell}^{(k)} + \sum_{\ell < m \leq j} (\sigma_m^{(k)})^{-2} B_{im}^{(k)} B_{\ell m}^{(k)}.$$

In this case, it is a short exercise to see that $\Theta_{i\ell}^{*(1)} \neq \Theta_{i\ell}^{*(2)}$ only if at least one of the following two statements hold:

1. $B_{i\ell}^{(1)} \neq B_{i\ell}^{(2)}$ or $\sigma_\ell^{(1)} \neq \sigma_\ell^{(2)}$;
2. There exists at least one of $\ell < m \leq j$ with $i \rightarrow m \leftarrow \ell$ in either $\mathcal{G}^{(1)}$ or $\mathcal{G}^{(2)}$ such that $B_{im}^{(1)} \neq B_{im}^{(2)}$ or $B_{\ell m}^{(1)} \neq B_{\ell m}^{(2)}$ or $\sigma_m^{(1)} \neq \sigma_m^{(2)}$.

By applying Assumption C.1, we have that $\Theta_{i\ell}^{*(1)} \neq \Theta_{i\ell}^{*(2)} \Rightarrow i, \ell \in S_\Theta$.

The diagonal entries of the precision matrix are given by:

$$\Theta_{ii}^{*(k)} = (\sigma_i^{(k)})^{-2} + \sum_{i < m \leq j} (\sigma_m^{(k)})^{-2} B_{im}^{(k)}.$$

Clearly, $\Theta_{ii}^{*(1)} \neq \Theta_{ii}^{*(2)}$ only if at least one of the following statements holds:

1. $\sigma_i^{(1)} \neq \sigma_i^{(2)}$;
2. $B_{im}^{(1)} \neq B_{im}^{(2)}$ or $\sigma_m^{(1)} \neq \sigma_m^{(2)}$ for at least one of the descendants of i in either $\mathcal{G}^{(1)}$ or $\mathcal{G}^{(2)}$ with $i < m \leq j$.

By applying Assumption C.1 we have that $\Theta_{ii}^{*(1)} \neq \Theta_{ii}^{*(2)} \Rightarrow i \in S_\Theta$. \square

Lemma C.4. *Under Assumption 4.1, given two linear SEMs $(B^{(1)}, \epsilon^{(1)})$ and $(B^{(2)}, \epsilon^{(2)})$, $B_{ij}^{(1)} = B_{ij}^{(2)}$ if and only if*

$$\exists S \subseteq S_\Theta \setminus \{i, j\} \text{ s.t. } \beta_{i,j|S}^{(1)} = \beta_{i,j|S}^{(2)} \text{ or } \beta_{j,i|S}^{(1)} = \beta_{j,i|S}^{(2)}.$$

Proof. To prove ‘‘if’’, we can prove the contrapositive, i.e. if $B_{ij}^{(1)} \neq B_{ij}^{(2)}$, then

$$\forall S \subseteq S_\Theta \setminus \{i, j\}, \beta_{i,j|S}^{(1)} \neq \beta_{i,j|S}^{(2)} \text{ and } \beta_{j,i|S}^{(1)} \neq \beta_{j,i|S}^{(2)}. \quad (\text{S.3})$$

It follows from Assumption 4.1 that Eq. (S.3) is true.

Now, we prove “only if”, i.e., if $B_{ij}^{(1)} = B_{ij}^{(2)}$, then

$$\exists S \subseteq S_\Theta \setminus \{i, j\} \text{ s.t. } \beta_{i,j|S}^{(1)} = \beta_{i,j|S}^{(2)} \text{ or } \beta_{j,i|S}^{(1)} = \beta_{j,i|S}^{(2)}.$$

We divide into two cases: $\sigma_j^{(1)} = \sigma_j^{(2)}$, and $\sigma_j^{(1)} \neq \sigma_j^{(2)}$.

Case 1 $\sigma_j^{(1)} = \sigma_j^{(2)}$

Consider the precision matrix $\Theta^{*(k)}$ of the random vector $X_{1:j}^{(k)}$. In this case, we prove that choosing the conditioning set as $S = S_{\Theta^*} \setminus \{i, j\}$ will give us regression invariance. This is a valid choice for S , since it is a subset of $S_\Theta \setminus \{i, j\}$ by Lemma C.3.

We will first show that $\Theta_{ij}^{*(1)} = \Theta_{ij}^{*(2)}$ and $\Theta_{jj}^{*(1)} = \Theta_{jj}^{*(2)}$. According to the new SEM of the marginal distribution of random vector $X_{1:j}^{(k)}$, i.e.,

$$X_{1:j}^{(k)} = (B_{1:j,1:j}^{(k)})^T X_{1:j}^{(k)} + \epsilon_{1:j}^{(k)},$$

it's easy to conclude that node j no longer has any descendants in the marginal SEM. We therefore have that

$$\Theta_{ij}^{*(k)} = -(\sigma_j^{(k)})^{-2} B_{ij}^{(k)} \quad \text{and} \quad \Theta_{jj}^{*(k)} = (\sigma_j^{(k)})^{-2}.$$

Since $B_{ij}^{(1)} = B_{ij}^{(2)}$ and $\sigma_j^{(1)} = \sigma_j^{(2)}$,

$$\Theta_{ij}^{*(1)} = \Theta_{ij}^{*(2)} \quad \text{and} \quad \Theta_{jj}^{*(1)} = \Theta_{jj}^{*(2)}. \quad (\text{S.4})$$

By choosing $M := S \cup \{i, j\}$ and denoting $M^* := [j] \setminus M$, recall that the entries of $\Theta_M^{(k)}$ can be written as:

$$(\Theta_M^{(k)})_{i_M j_M} = \Theta_{ij}^{*(k)} - \Theta_{i, M^*}^{*(k)} (\Theta_{M^*, M^*}^{*(k)})^{-1} \Theta_{M^*, j}^{*(k)}.$$

Now, by invoking Lemma C.2 and Eq. (S.4), $(\Theta_M^{(1)})_{i_M j_M} = (\Theta_M^{(2)})_{i_M j_M}$ and $(\Theta_M^{(1)})_{j_M j_M} = (\Theta_M^{(2)})_{j_M j_M}$. Finally, using Eq. (S.2), we have $\beta_{i,j|S}^{(1)} = \beta_{i,j|S}^{(2)}$.

Case 2 $\sigma_j^{(1)} \neq \sigma_j^{(2)}$

In this case, we prove that regressing on all of the parents of j in both DAGs, i.e., choosing the conditioning set as $S = \text{Pa}^{(1)}(j) \cup \text{Pa}^{(2)}(j) \setminus \{i\}$, will give us regression invariance. This is a valid choice for S , i.e. $S \subseteq S_\Theta \setminus \{i, j\}$, since Assumption C.1 ensures that $\sigma_j^{(1)} \neq \sigma_j^{(2)} \Rightarrow \forall \ell \in \text{Pa}^{(k)}(j), \ell \in S_\Theta$.

Let $M := S \cup \{i\}$. By regressing $X_j^{(k)}$ onto $X_M^{(k)}$, we get the regression coefficient as

$$X_j^{(k)} = (\beta_M^{(k)})^T X_M^{(k)} + \tilde{\epsilon}_j^{(k)}.$$

Let $(\beta_M^{(k)})_{\ell_M}$ denote the ℓ_M -th entry of $\beta_M^{(k)}$. By the Markov property, when regressing $X_j^{(k)}$ onto $X_M^{(k)}$ where

$\text{Pa}^{(k)}(j) \subseteq M \subseteq [j-1]$, it is guaranteed that $(\beta_M^{(k)})_{\ell_M} = B_{\ell j}^{(k)}$ if $\ell \in \text{Pa}^{(k)}(j)$ and $(\beta_M^{(k)})_{\ell_M} = 0$ otherwise. Therefore, we have that $\beta_{i,j|S}^{(k)} = (\beta_M^{(k)})_{i_M} = B_{ij}^{(k)}$, which completes the proof. \square

Then we get the proof of Theorem 4.3 as:

Proof. By applying Assumption C.1 we have that $\bar{\Delta} \subseteq \Delta_\Theta$. Then the proof of Theorem 4.3 follows trivially from Lemma C.4, since Lemma C.4 shows that edge $i-j$ would be deleted during testing the invariance of regression coefficients if and only if $i-j \notin \bar{\Delta}$. \square

We end this section with a remark about the strength of Assumption C.1.

Remark C.5 (Strength of Assumption C.1). *To analyze the strength of Assumption C.1, consider instead the following stronger assumption:*

Assumption C.1' *For any choices of $i, j \in [p]$, it holds that*

1. *If $B_{ij}^{(1)} \neq B_{ij}^{(2)}$, then $\Theta_{ij}^{(1)} \neq \Theta_{ij}^{(2)}$, and $\Theta_{i\ell}^{(1)} \neq \Theta_{i\ell}^{(2)}$ for any ℓ with directed path $i \rightarrow j \leftarrow \ell$ in either $\mathcal{G}^{(1)}$ or $\mathcal{G}^{(2)}$.*
2. *If $\sigma_j^{(1)} \neq \sigma_j^{(2)}$, then $\Theta_{jj}^{(1)} \neq \Theta_{jj}^{(2)}$, and $\Theta_{ii}^{(1)} \neq \Theta_{ii}^{(2)} \forall i \in \text{Pa}^{(1)}(j) \cup \text{Pa}^{(2)}(j)$.*

Assumption C.1' is a strictly stronger assumption than Assumption C.1, i.e., Assumption C.1 is satisfied whenever Assumption C.1' is satisfied. We expect Assumption C.1' to be much weaker than Assumptions 4.1 and 4.2 in the finite sample regime, and therefore the same also holds for Assumption C.1. This is because the number of hypersurfaces violating Assumption C.1' scales at most $\mathcal{O}(p^4)$, which is a much smaller number as compared to Assumptions 4.1 and 4.2 that scale as $\mathcal{O}(|\Delta_\Theta|2^{|S_\Theta|-1})$. We therefore claim that Assumption C.1' is much weaker in the finite sample regime. \square

C.3. Proof of Theorem 4.4

In this section, we give proof of Theorem 4.4 when Algorithm 3 is initialized with difference-UG.

Lemma C.6. *For all nodes j incident to at least one edge in $\bar{\Delta}$, $\sigma_j^{(1)} = \sigma_j^{(2)} \Leftrightarrow \exists S \subseteq S_\Theta \setminus \{i, j\}$ s.t. $\sigma_{j|S}^{(1)} = \sigma_{j|S}^{(2)}$.*

Proof. To prove “if”, it is equivalent to proving that, if $\sigma_j^{(1)} \neq \sigma_j^{(2)}$, then

$$\forall S \subseteq S_\Theta \setminus \{j\}, \sigma_{j|S}^{(1)} \neq \sigma_{j|S}^{(2)}. \quad (\text{S.5})$$

It follows from Assumption 4.2 that Eq. (S.5) is true.

To prove “only if”, consider again the marginal distribution of $X_{1:j}^{(k)}$. Since $\sigma_j^{(1)} = \sigma_j^{(2)}$, we have that $\Theta_{jj}^{*(1)} = \Theta_{jj}^{*(2)}$. Let $M := S_{\Theta^*} \cup \{j\}$ and let $S := M \setminus \{j\}$, since $(\sigma_{j|S}^{(k)})^2 = ((\Theta_M^{(k)})_{jMjM})^{-1}$ and $(\Theta_M^{(1)})_{jMjM} = (\Theta_M^{(2)})_{jMjM}$ by using Lemma C.2, we have that $\sigma_{j|S}^{(1)} = \sigma_{j|S}^{(2)}$. \square

Lemma C.7. $\forall i - j \in \bar{\Delta}$ such that $\sigma_j^{(1)} = \sigma_j^{(2)}$ it holds that,

1. if $i \rightarrow j \in \Delta$, then $i \in S \forall S$ s.t. $\sigma_{j|S}^{(1)} = \sigma_{j|S}^{(2)}$.
2. if $j \rightarrow i \in \Delta$, then $i \notin S \forall S$ s.t. $\sigma_{j|S}^{(1)} = \sigma_{j|S}^{(2)}$.

Proof. We prove both statements by contradiction. For $B_{ij}^{(1)} \neq B_{ij}^{(2)}$, suppose there exists a S such that $\sigma_{j|S}^{(1)} = \sigma_{j|S}^{(2)}$ while $i \notin S$. This contradicts Assumption 4.2.

Similarly, in the second statement for $B_{ji}^{(1)} \neq B_{ji}^{(2)}$, suppose there exists S such that $\sigma_{j|S \cup \{i\}}^{(1)} = \sigma_{j|S \cup \{i\}}^{(2)}$. This also contradicts Assumption 4.2. \square

Then the formal proof of Theorem 4.4 is as follows:

Proof. By Lemma C.6, there exists S such that

$$\sigma_{j|S}^{(1)} = \sigma_{j|S}^{(2)}$$

if and only if $\sigma_j^{(1)} = \sigma_j^{(2)}$. Therefore, only the nodes where the internal noise variance is unchanged will be chosen by Algorithm 3. In addition, it also follows from Lemma C.7 that for any $i \rightarrow j \in \Delta$, $i \in S$ and for any $j \rightarrow i \in \Delta$, $i \notin S$. \square

D. Examples for Remark 4.7

Since our assumptions are closely related to the faithfulness assumption, it is interesting to compare the entailment relationship between our assumptions, i.e., Assumptions 4.1 and 4.2, and the faithfulness assumption. In this section, we give the following two counterexamples to show that our assumptions and the faithfulness assumption do not imply one another. Therefore, the assumptions proposed in our paper are not comparable with the faithfulness assumption.

Example D.1. We give a 3-node example that satisfies Assumptions 4.1 and 4.2 but does not satisfy the faithfulness assumption. Consider two linear SEMs $(B^{(1)}, \epsilon^{(1)})$ and $(B^{(2)}, \epsilon^{(2)})$ with $\epsilon_j^{(k)} \sim \mathcal{N}(0, 1) \forall j, k$. Let $B^{(1)}$ and $B^{(2)}$ be the autoregressive matrices defined as shown in Figure D.1. Clearly, $\mathbb{P}^{(1)}$ does not follow the faithfulness assumption with respect to $\mathcal{G}^{(1)}$ since node 1 and 3 are d -connected given \emptyset , but $X_1^{(1)} \perp\!\!\!\perp X_3^{(1)}$. However, it is a short exercise to show that for all choices of S , i.e. \emptyset and

$\{2\}$, we have $\beta_{1,3|S}^{(1)} \neq \beta_{1,3|S}^{(2)}$, $\beta_{3,1|S}^{(1)} \neq \beta_{3,1|S}^{(2)}$, $\sigma_{3|S}^{(1)} \neq \sigma_{3|S}^{(2)}$ and $\sigma_{1|S \cup \{3\}}^{(1)} \neq \sigma_{1|S \cup \{3\}}^{(2)}$. Therefore, this example satisfies Assumptions 4.1 and 4.2.

Example D.2. We give a 3-node example that satisfies the faithfulness assumption but does not satisfy Assumption 4.1. Consider two linear SEMs where all $\epsilon_j^{(k)}$ are standard normal random variables and $B^{(1)}$ and $B^{(2)}$ are defined as shown in Figure D.2. Although $B_{13}^{(1)} \neq B_{13}^{(2)}$, by choosing $S = \emptyset$, we still have that $\beta_{1,3|S}^{(1)} = \beta_{1,3|S}^{(2)} = 0.5$. Therefore, although both SEMs satisfy the faithfulness assumption, the pair does not satisfy Assumption 4.1.

E. Constraint-based method for estimating difference-UG

In this section, we present a constraint-based method for estimating the difference-UG model when noise terms of the underlying linear SEMs are general noises (not necessarily Gaussian). Our constraint-based method is built on performing hypothesis test on each (i, j) -th entry and then find the set of (i, j) -th entries where $\Theta_{ij}^{(1)} \neq \Theta_{ij}^{(2)}$. The test for invariance of diagonal entries, i.e., $\Theta_{ii}^{(k)}$, is equivalent to the hypothesis test $H_0^{i|[p] \setminus \{i\}}$ as discussed in Section 3, since $(\sigma_{i|[p] \setminus \{i\}}^{(k)})^2 = (\Theta_{ii}^{(k)})^{-1}$. For the non-diagonal entries, since the non-zero pattern of $\Theta_{ij}^{(k)}$ is the same as the non-zero pattern of the partial correlation coefficients, i.e., $\rho_{ij|[p] \setminus \{i, j\}}^{(k)}$, we first find the set of non-diagonal entries that

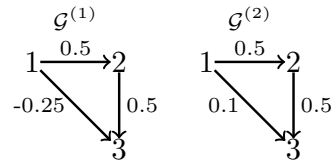


Figure D.1. Example of two linear SEMs that satisfy Assumptions 4.1 and 4.2 but do not satisfy the faithfulness assumption. The autoregressive matrices $B^{(1)}$ and $B^{(2)}$ are shown as edge weights in $\mathcal{G}^{(1)}$ and $\mathcal{G}^{(2)}$. We assume all noise terms are standard normal random variables.

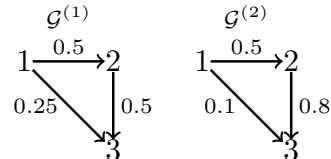
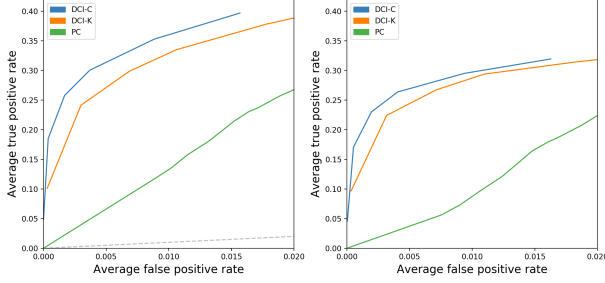


Figure D.2. Example of two linear SEMs that satisfy the faithfulness assumption but do not satisfy Assumption 4.1. The autoregressive matrices $B^{(1)}$ and $B^{(2)}$ are shown as edge weights in $\mathcal{G}^{(1)}$ and $\mathcal{G}^{(2)}$. We assume all noise terms are standard normal random variables.



(a) difference-DAG skeleton $\bar{\Delta}$ (b) difference-DAG Δ

Figure F.1. ROC curves for estimating the difference-DAG Δ and its skeleton $\bar{\Delta}$ with $p = 100$ nodes, expected neighbourhood size $s = 10$, $n = 300$ samples, and 10% percent change between DAGs.

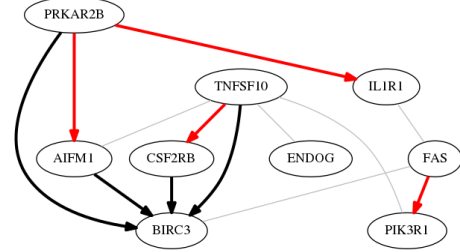
are different between $\Theta^{(1)}$ and $\Theta^{(2)}$ by doing partial correlation tests for each distribution and then comparing the non-zero patterns. After that, for each entry (i, j) that is estimated to be non-zero in both $\Theta^{(1)}$ and $\Theta^{(2)}$, we use the test statistic:

$$\hat{Q} := \left(\hat{\Theta}_{ij}^{(1)} - \hat{\Theta}_{ij}^{(2)} \right)^2 \cdot \left(\frac{\hat{\Theta}_{ii}^{(1)} \hat{\Theta}_{jj}^{(1)} + (\hat{\Theta}_{ij}^{(1)})^2}{n_1} + \frac{\hat{\Theta}_{ii}^{(2)} \hat{\Theta}_{jj}^{(2)} + (\hat{\Theta}_{ij}^{(2)})^2}{n_2} \right)^{-1}$$

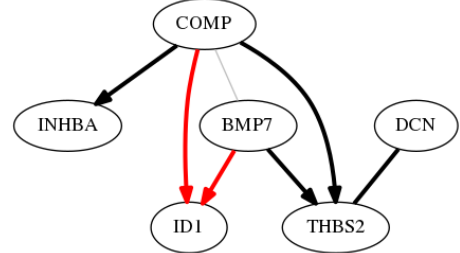
and test if it fits the F-distribution with parameters $F(1, n_1 + n_2 - 2p + 2)$. If the hypothesis is true, then we take this entry as invariant between the two precision matrices. The consistency guarantee of $H_0^{i|[p]\setminus\{i\}}$ and partial correlation tests follows trivially from the previous results. For \hat{Q} , it follows from Proposition 3 of (Drton & Perlman, 2007) on the asymptotic normal distribution of the empirical precision matrix $\hat{\Theta}$ that if the null hypothesis is true, \hat{Q} would converge in distribution to $\chi^2(1)$ as $n_1, n_2 \rightarrow \infty$. Following our previous claim on \hat{T} , \hat{Q} is also consistent.

F. Additional high-dimensional evaluation

High-dimensional setting: 10% changes. We present the results of increasing the number of changes between the two DAGs, and hence the size of S_Θ . We used the same simulation parameters as we use for Figure 3, i.e. $p = 100$ nodes, a neighbourhood size of $s = 10$, and sample size $n = 300$, except that the total number of changes was 10% of the number of edges in $B^{(1)}$, rather than 5%. As shown in Figure F.1, both initializations of the DCI algorithm still outperform separate estimation by the PC algorithm. However, because the underlying DAGs have maintained constant sparsity while the difference-DAG has become more dense, the gains in performance by using the DCI algorithm have slightly diminished, as expected by our theoretical analysis.



(a) Apoptosis pathway



(b) TGF- β pathway

Figure G.1. Estimate of the difference DAG model between the two groups for apoptosis pathway and TGF- β pathway. Here the black lines corresponds to the edges discovered by both our method and DPM, the red lines are the edges discovered only by our method, the grey lines are the undirected edges discovered only by DPM.

G. Real data analysis - ovarian cancer

We tested our method on an ovarian cancer data set (Tohill et al., 2008). This data set consists of the gene expression data of patients with ovarian cancer. The patients are divided into six subtypes (C1-C6). The C1 subtype was characterized by differential expression of genes associated with stromal and immune cell types and has much shorter survival rate. In this experiment, we divide the subjects into two groups, group 1 with $n_1 = 78$ subjects containing patients with C1 subtype, and group 2 with $n_2 = 113$ subjects containing patients with C2-C6 subtypes. In this work, we focused on two pathways from the KEGG database (Ogata et al., 1999; Kanehisa et al., 2011), the apoptosis pathway containing 87 genes, and the TGF- β pathway with 82 genes.

We compare our results to those obtained by the DPM method (Zhao et al., 2014), which infers the difference graph. As input to Algorithm 2, we take S_Θ to be all of the nodes in the output of the DPM algorithm and take Δ_Θ to be the fully connected graph on S_Θ . We then learn the difference DAG using Algorithm 3. The final set of edges over different tuning parameters was chosen using stability selection as recommended by (Meinshausen & Bühlmann, 2010) and is shown in Figure G.1. We identify two hub nodes in the apoptosis pathway: BIRC3 and PRKAR2B. BIRC3 has been shown to be an inhibitor of apoptosis (Johnstone et al., 2008) and is one of the top deregulated genes in ovarian

cancer (Jönsson et al., 2014). This gene has also been recovered by the DPM method as one of the hub nodes. While BIRC3 has high in-degree, hub gene PRKAR2B has high out-degree, making it a better candidate for possible interventions in ovarian cancer since knocking out a gene with high out-degree will have widespread downstream effects on the target genes. Indeed, PRKAR2B is an important regulatory unit for cancer cell growth (Chiaradonna et al., 2008) and the RII- β protein encoded by PRKAR2B has also been well studied as a therapeutic target for cancer therapy (Mikalsen et al., 2006; Cho-Chung, 1999). In addition, PRKAR2B has also been shown to play a very important role in disease progression in ovarian cancer cells (Cheadle et al., 2008). Since the DPM method does not infer directionality, it is not possible to tell which of the hub genes might be a better interventional target. An advantage of our method is that we are able to identify possible therapeutic targets in real data, as showcased by finding an existing drug target for cancer.

For the TGF- β pathway, we find THBS2 and COMP to be the hub nodes. Both of these genes have been implicated in resistance to chemotherapy in epithelial ovarian cancer (Marchini et al., 2013), confirming the importance of our findings. These nodes were also recovered by DPM.

Overall, the UG discovered by DPM is comparable to the DAG found by our method. In fact, the disparity in the TGF- β pathway between the difference UG model Δ_{Θ} and the difference DAG model Δ can be explained by the fact that the edge between COMP–BMP7 in Δ_{Θ} can be accounted for by the two edges BMP7 \rightarrow ID1 and COMP \rightarrow ID1 in Δ . Though these edges might represent the true regulatory pathways affected, the sparsity-inducing penalty in the DPM algorithm could remove them while leaving the edge between COMP and BMP7. This disparity between the two algorithms highlights the importance of replacing correlative reasoning with causal reasoning, and accentuates the significance of our contribution.